Energy Technology
Generation, Conversion, Storage, Distribution
www.entechnol.de

Check for updates

Solid versus Liquid—A Bottom-Up Calculation Model to Analyze the Manufacturing Cost of Future High-Energy Batteries

Joscha Schnell, Heiko Knörzer, Anna Julia Imbsweiler, and Gunther Reinhart*

All-solid-state batteries (ASSB) are promising candidates for future energy storage. However, only a little is known about the manufacturing costs for industrial production. Herein, a detailed bottom-up calculation is performed to estimate the required investment and to facilitate comparison with conventional lithium-ion batteries (LIB). Results indicate that sulfide-based ASSBs can indeed be competitive if the material compatibility issues can be solved and production is successfully scaled. In contrast, oxide-based ASSBs will probably not be able to compete if cost is the decisive factor. A sensitivity analysis with Monte Carlo simulation reveals that the inert gas atmosphere required for sulfide-based ASSBs contributes little to the overall cell costs, whereas the sintering step for oxide-based ASSBs is highly critical. The calculation also indicates that in-house manufacturing of the lithium anode will be cheaper than purchasing the lithium foil externally if the cell producer has sufficient processing know-how. Finally, the aerosol deposition method is investigated, revealing that a deposition rate far above 1000 mm^3 min^{-1} would be required to make the technology economically feasible in ASSB production. The results of this study will help researchers and industry prioritize development efforts and push the scale-up of future high-energy batteries with improved performance.

1. Introduction

Efficient means of energy storage are required to tackle the issues associated with the transfer from fossil fuels to renewable energies and electro mobility. All-solid-state batteries (ASSB) represent the next frontier toward lithium-based batteries with improved performance: The replacement of the flammable liquid electrolyte by a nonflammable solid electrolyte (SE) could lead to better safety characteristics of ASSBs compared with conventional lithium-ion batteries (LIBs).[1] Furthermore, a dense solid electrolyte separator (SES) membrane could facilitate the use of a lithium metal anode for higher energy density,[2] and the high ionic conductivity of some SE materials could facilitate fast charging and high power.[3] Among the most promising material systems are sulfide-based SEs, such as Li_2S–P_2S_5 (LPS),[4] and oxide-based SEs, such as $Li_{1.3}Al_{0.3}Ti_{1.7}(PO_4)_3$ (LATP)[5] or $Li_7La_3Zr_2O_{12}$ (LLZ).[6] Although encouraging results have been achieved in laboratory applications, reports on up-scaling toward larger cell formats with competitive energy densities remain scarce. Associated with the transfer from laboratory to pilot and industrial scale comes a large variety of risks (**Figure 1**a), from raw materials sourcing,[7] unclear cell design,[8] fabrication issues,[9,10] up to battery operation, and end of life. The rapidly falling costs of conventional LIBs[11,12] make an investment into a new technology, such as the ASSB, a highly critical endeavor. Hence, an elaborate economic assessment is required to determine whether ASSBs can potentially be fabricated at costs competitive to conventional LIBs.

To date, not many publications have dealt with economic aspects of ASSBs. A direct comparison with conventional LIBs has turned out to be challenging due to the high uncertainty associated with the material cost for ASSBs, in particular, the lithium metal price and the SE cost.[14] A recent top-down calculation for oxide-based ASSB indicated that fabrication cost could become competitive due to numbers of scale.[15] However, important questions on the cost associated with specific production issues, such as the inert gas atmosphere needed for processing of sulfide-based SEs[16] and the high sintering temperatures (>1000 °C) required for oxide-based SEs to achieve sufficient ionic conductivity,[17] remain unanswered.

Therefore, this study investigates different scenarios for mass production of ASSBs from an economic perspective to enable a comparison with conventional LIB cell production. For this purpose, a bottom-up calculation tool for battery production cost modeling was built (Figure 1b, cf. Section 3). This allows to investigate the economic impact of different cell designs and varying material costs for sulfide- and oxide-based ASSBs, as well as innovative processing technologies, such as the aerosol deposition method (ADM). By providing an in-depth

J. Schnell, H. Knörzer, A. J. Imbsweiler, Prof. G. Reinhart
Department of Mechanical Engineering
Institute for Machine Tools and Industrial Management
Technical University of Munich
Boltzmannstr. 15, 85748 Garching, Germany
E-mail: joscha.schnell@iwb.mw.tum.de

The ORCID identification number(s) for the author(s) of this article can be found under https://doi.org/10.1002/ente.201901237.

© 2020 The Authors. Published by WILEY-VCH Verlag GmbH & Co. KGaA, Weinheim. This is an open access article under the terms of the Creative Commons Attribution License, which permits use, distribution and reproduction in any medium, provided the original work is properly cited.

DOI: 10.1002/ente.201901237

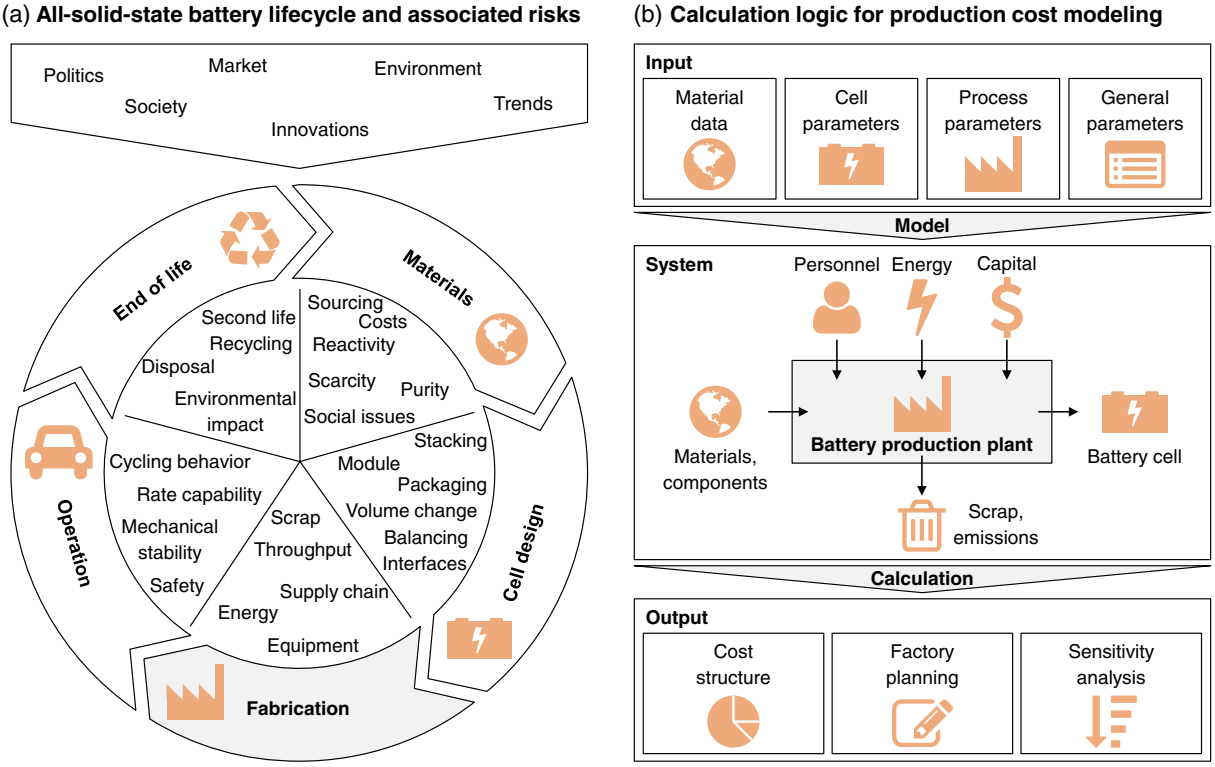

Figure 1. a) External influences on the ASSB lifecycle and associated risks from raw materials to cell design, fabrication, operation, and end of life. b) Bottom-up calculation logic for battery production cost modeling, as suggested by Schünemann[13].

analysis on critical process steps and bottlenecks in ASSB production from a bottom-up perspective, this study will help researchers and decision makers to plan the next steps toward better batteries with increased safety.

2. Results and Discussion

2.1. Liquid versus Solid Electrolyte

For ASSBs to be competitive in the market, the overall cost must be comparable to the cost of conventional LIBs. However, due to the low maturity degree of ASSBs, a realistic comparison should also take into account future advances of the conventional LIB technology, in particular, with regard to anode development.[18] **Figure 2**a shows a comparison of different cell designs for LIBs with graphite and Si/C anode, and for sulfide-based ASSBs with graphite anode (solid-state LIB, SLIB) and lithium anode (solid-state lithium metal battery, SLMB). To ensure comparability, the cathode area specific capacity was held constant for all scenarios at 5.64 mAh cm^{-2}, corresponding to a 100 µm thick $LiNi_{0.8}Co_{0.1}Mn_{0.1}O_2$ (NMC 811) cathode with an active material (AM) content of 60 vol%. Each cathode contains 5 vol% binder and 5 vol% conductive agent (CA), whereas the remaining 30 vol% are taken up either by liquid or SE ("catholyte"). The anode thickness was adjusted to fit the area specific capacity of the cathode, with a balancing factor of 1.1 for the graphite and Si/C anode[14] (to ensure all lithium drawn from the cathode can be stored) and a 50% surplus for the lithium metal anode[2] (to account for irreversible losses during cycling). The separator thickness was set to 20 µm for all scenarios. The cell design parameters for cathode, separator, and anode are summarized in **Table 1**. A 15 µm thick aluminum current collector and a 10 µm thick copper current collector were assumed for cathode and anode, respectively. The energy density and specific energy were calculated on the cell level for a plug-in hybrid electric vehicle (PHEV) cell format (type 2)[19] with a volume utilization of 85% and appropriate overlap for separator, anode, and cathode (cf. Table S1, Supporting Information).[13] As to be expected,[2] the LIB and SLIB with graphite anode show the lowest energy density (530 Wh L^{-1}), with a slightly lower specific energy of the SLIB due to the higher density (cf. Table S2, Supporting Information) of the LPS SE (2 g cm^{-3}) in contrast to the liquid electrolyte (1.3 g cm^{-3}).[18] Due to the higher specific capacities of Si/C (1000 mAh g^{-1})[20] and Li (3862 mAh g^{-1}),[21] the respective anode thicknesses (and mass) can be decreased. Hence, more galvanic cells (cathode, separator, anode) can be fit into one PHEV cell housing, resulting in a higher energy density and specific energy.[18]

To estimate the manufacturing cost for the different cell designs, a mass production scenario with an annual output of 6 GWh[22] was simulated. Note that a running production with three shifts per day (cf. Supplementary Table S3, Supporting Information) is assumed for the simulation and additional cost for production ramp-up is not taken into account. Due to the different energy content of the respective battery cell types, the number of cells to be produced per year varies from 19.7 million for the SLMB with lithium anode and 24.9 million for the LIB

© 2020 The Authors. Published by WILEY-VCH Verlag GmbH & Co. KGaA, Weinheim

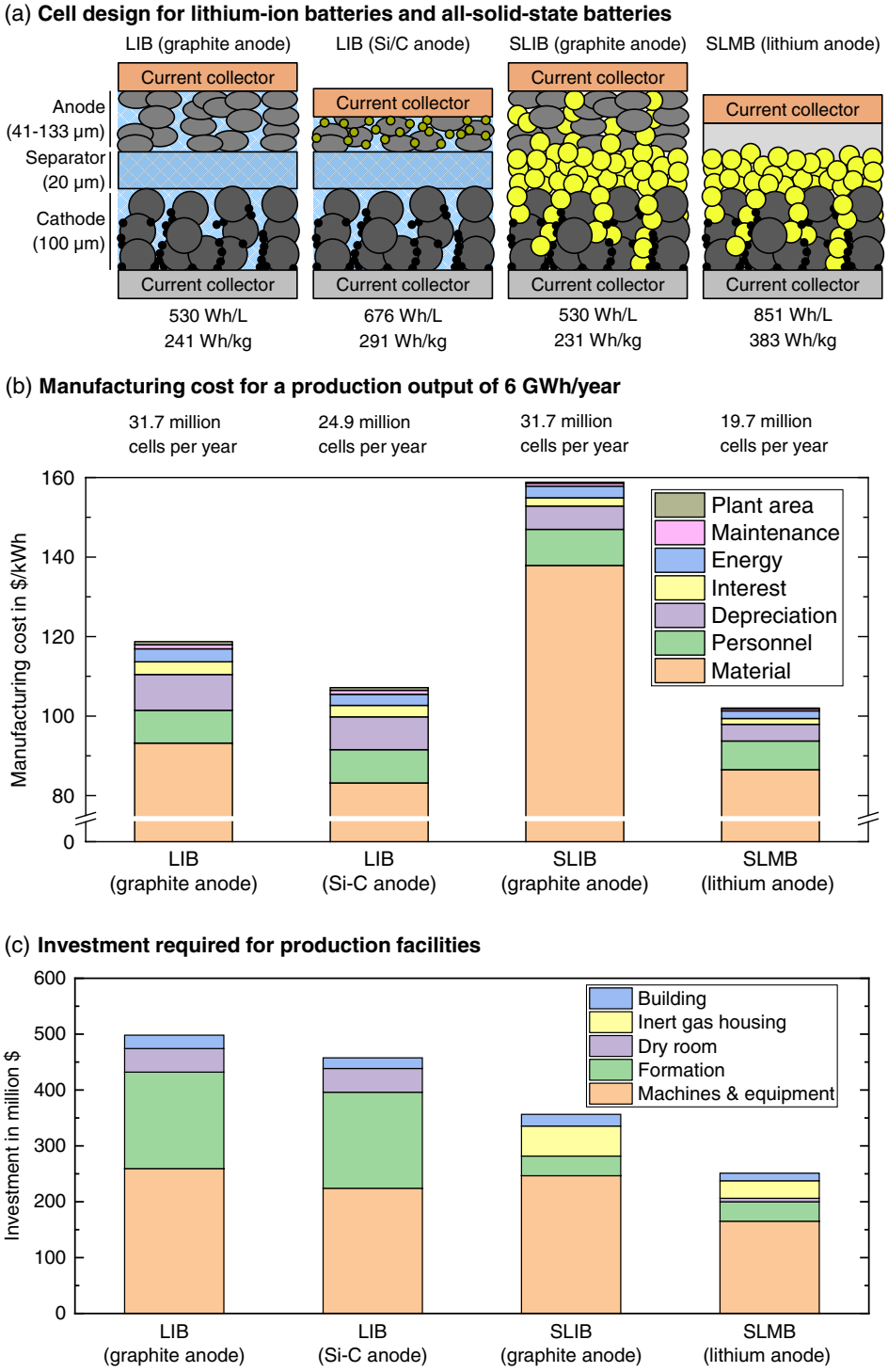

Figure 2. a) Cell design for different types of LIBs and all-solid-state lithium-ion and lithium metal batteries (SLIB/SLMB) with a sulfide-based SE. Calculations for energy density (in Wh L^{-1}) and specific energy (in Wh kg^{-1}) are on the cell level (incl. PHEV 2 housing) for an NMC 811 cathode area specific capacity of 5.64 $mAhcm^{-2}$ (cf. main text). b) Number of PHEV cells to be produced for the different scenarios and corresponding manufacturing cost, as well as c) required investment for an output of 6 GWh per year.

with Si/C anode up to 31.7 million for the LIB and SLIB with graphite anode. Typically, a wet coating procedure is assumed for the electrodes, i.e., a homogeneous slurry is cast directly onto the current collector foil and the solvent is evaporated in a drying tunnel.[23] The porosity of the resulting layer is reduced by a calendering step,[24] before slitting the resulting coil into several

© 2020 The Authors. Published by WILEY-VCH Verlag GmbH & Co. KGaA, Weinheim

Table 1. Thickness and composition of the components for the scenarios depicted in Figure 2a. The cathode composition was calculated for 60 vol% AM, 5 vol% binder, 5 vol% CA, and 30 vol% porosity (LIB) or catholyte (SLIB/SLMB). The SLIB/SLMB separator composition was calculated for 95 vol% SE and 5 vol% binder. The graphite (Si/C) anode composition was calculated for 60 (45) vol% AM, 5 (5) vol% binder, and 30 (50) vol% porosity (or anolyte). The thicknesses do not include current collectors (cf. main text).

Component		LIB [graphite anode]		LIB [Si/C anode]		SLIB [graphite anode]		SLMB [Li anode]	
			wt%		wt%		wt%		wt%
Cathode	Thickness	100 µm		100 µm		100 µm		100 µm	
	AM	NMC 811	93.75	NMC 811	93.75	NMC 811	78.99	NMC 811	78.99
	Binder	PVDF	2.93	PVDF	2.93	NBR	1.40	NBR	1.40
	CA	CB	3.32	CB	3.32	CB	2.80	CB	2.80
	Catholyte	–	–	–	–	LPS	16.81	LPS	16.81
	Porosity	30 vol%	–	30 vol%	–	–	–	–	–
Separator	Thickness	20 µm		20 µm		20 µm		20 µm	
	Separator	PO	100	PO	100	LPS	97.44	LPS	97.44
	Binder	–	–	–	–	NBR	2.56	NBR	2.56
	Porosity	40 vol%	–	40 vol%	–	–	–	–	–
Anode	Thickness	133 µm		61 µm		133 µm		41 µm (charged[a])	
	AM	Graphite	94.83	Si/C	94.85	Graphite	67.81	Li	100
	Binder	SBR	5.17	SBR	5.15	NBR	3.36	–	–
	Anolyte	–	–	–	–	LPS	28.83	–	–
	Porosity	30 vol%	–	50 vol%	–	–	–	–	–

[a]Note that only the excess lithium (50%) is inserted into the cell during cell assembly, corresponding to a lithium foil thickness of 14 µm. During charge of the battery, the lithium anode will expand by 27 µm due to the lithium plated from the cathode.

slimmer coils. Main difference for the SLIB is the SES, which can be coated directly onto one of the electrode layers.[25] In contrast, for the SLMB, an extrusion step is assumed for fabrication of the lithium anode. The resulting lithium foil is rolled using a calender to achieve the desired thickness before lamination onto the current collector and slitting to width. During cell assembly, electrode sheets are cut to size and stacked (typically by flat winding, z-folding, or single sheet stacking),[26] before tab welding and packaging. For the conventional lithium-ion cells, the liquid electrolyte is filled into the cell[27] before cell formation, storage, and final quality check. The corresponding process parameters are summarized in Table S4, Supporting Information. All other input parameters for the different scenarios can be found in Table S1–S3, Supporting Information.

Special attention should be paid to the environmental conditions for processing of the different components: For the LIBs with liquid electrolyte, fabrication of the graphite and Si/C anode can take place in a normal production environment, whereas the moisture sensitivity of the NMC 811 cathode[28] and the liquid electrolyte necessitates cathode fabrication and cell assembly in a dry room.[29] Similarly, fabrication of the lithium anode requires dry atmosphere to hinder unwanted degradation or spontaneous ignition.[30] In contrast, an inert gas housing (glovebox) will be required for all process steps involving the sulfide-based SE[9] due to the risk of toxic H_2S formation.[16] The modeling parameters for dry room and inert gas housing are summarized in **Table 2**. The dry room area was assumed to take up 4.4 times the machine base area (considering additional space for intralogistics and intermediate storage, etc.),[13] whereas the glovebox volume was calculated based on the machine base area multiplied by an average enclosure height of 1.50 m.

Table 2. Input parameters for dry room and glove box equipment. Dry room parameters were taken from Schünemann,[13] glove box parameters were averaged from a quotation by a glove box manufacturer for encapsulation of a LIB cell production line. Values given in € were calculated at a conversion rate of 1.15.

	Input parameter	Unit	Value
Dry room	Investment	$ m^{-2}	5721.25
	Depreciation period	Years	15
	Average electrical power	kWh d^{-1} m^{-2}	6.8
	Industry energy price	$ kWh^{-1}	0.21
Glove box	Average price inert gas housing	$ m^{-3}	9639.81
	Average price gas purifier (incl. sensors)	$ m^{-3}	3050.12
	Price vacuum lock (800 mm + 150 mm + vac. pump)	$ per piece	48 501.25
	Depreciation period	Years	8
	Average gas loss	vol% h^{-1}	0.05
	Argon price	$ m^{-3}	2.30

A direct comparison of the manufacturing cost and required investment for the different cell designs is given in Figure 2b,c. Please note that the calculated values should not be considered absolute, but rather serve to enable a comparison of the different scenarios (cf. Section 3). Material costs are dominating (>75%)

© 2020 The Authors. Published by WILEY-VCH Verlag GmbH & Co. KGaA, Weinheim

for all cell designs, which is typical for lithium-ion cell production.[29] The material cost for the conventional LIB with graphite anode sum up to 93.2 \$ kWh^{-1}, whereas the processing costs (personnel, depreciation, interest, energy, maintenance, and plant area cost) only take up to 25.5 \$ kWh^{-1}. As predicted in a recent study by Schmuch et al., the material cost for the LIB with Si-C (83.2 \$ kWh^{-1}) are lower than for all other scenarios. However, the processing costs (24.0 \$ kWh^{-1}) are only slightly lower than for the graphite-based LIB, resulting in an overall manufacturing cost of 107.2 \$ kWh^{-1}. The highest material costs are obtained for the sulfide-based SLIB with graphite anode (137.9 \$ kWh^{-1}), whereas processing costs (20.9 \$ kWh^{-1}) are lower than for the LIBs with liquid electrolyte. Although the material costs for the SLMB with Li anode (86.5 \$ kWh^{-1}) are slightly higher than for the LIB with Si/C anode, the overall manufacturing costs (102.0 \$ kWh^{-1}) are lower due to the lowest processing cost of all cell designs (15.5 \$ kWh^{-1}).

To understand the underlying cost structure and required investment, the manufacturing costs for the four scenarios were clustered in **Figure 3** according to the individual cell components and production stages (electrode and separator manufacturing, cell assembly, and cell formation and test). As for the SLIB and SLMB, the SE is already mixed into the cathode slurry, the overall cathode material costs are higher compared with the conventional LIBs with liquid electrolyte. The slightly higher cathode processing costs for the SLIB (4.6 \$ kWh^{-1}) in comparison with the conventional LIBs (4.1–4.3 \$ kWh^{-1}) are mainly governed by the shorter depreciation period[31] for the glovebox environment (19 million dollars over a period of 8 years) in comparison with the dry room (22 million dollars over a period of 15 years). The cathode processing cost of the SLMB are lower (3.8 \$ kWh^{-1}) because the smaller number of cells to be produced requires one coating machine less. The anode material costs show the largest deviation. Here again, the additional SE for the SLIB results in the highest overall anode cost. In contrast, the Li anode material costs are even lower than for the Si/C anode, which is in good agreement with previous work.[14] More interestingly, the lithium extrusion and calendering process results in a significantly lower processing cost (1.4 \$ kWh^{-1}) in comparison with the wet coating processes for the other cell formats (4.1–4.7 \$ kWh^{-1}). The overall separator manufacturing cost (material and processing) for the SLIB (14.1 \$ kWh^{-1}) and SLMB (13.6 \$ kWh^{-1}) are higher than for the conventional LIB cells (9.6–10.3 \$ kWh^{-1}), where the separator is typically purchased by an external supplier. Both material and processing cost for cell assembly are lower for the SLIB and SLMB because the cumbersome electrolyte filling step can be omitted. Furthermore, the number of cells to be produced is decisive for the amount of PHEV housings required, resulting in lower cost for the LIB with Si/C anode in comparison with the graphite anode, and lower costs for the SLMB in comparison with the SLIB. The formation, aging, and final cell testing procedures significantly contribute to the processing cost for conventional LIBs due to the high investment for the formation channels and the large production space required for the testing and storage procedures.[32] Hence, by replacing the formation cycles[33] with a significantly shorter check-up procedure (cf. Section 3), processing costs for formation, storage, and testing can be reduced from 7.6–8.3 \$ kWh^{-1} for the conventional LIBs to 3.0–4.0 \$ kWh^{-1} for SLIB and SLMB.

Despite the overall lower processing cost for the SLIB with graphite composite anode, the high material cost will make this concept hardly feasible in a cost competitive market (such as the automotive industry), unless SE material cost can be pushed far below the assumed 50 \$ kg^{-1} for LPS.[14] The direct comparison of the LIB with Si/C anode and the SLMB with lithium anode reveals the cost savings potential for ASSB processing which could, with the underlying assumptions, compensate for the higher material cost. As to be expected, the electrolyte filling and formation procedures are among the main bottlenecks for conventional LIB production.[32] However, it should be noted that the assumptions are subject to a high degree of uncertainty and a deeper understanding of the ASSB processing steps will be required.

2.2. Lithium Foil—Make or Buy?

As deduced by Figure 2c, a significant cost savings potential results from reduced effort for lithium anode manufacturing in comparison to conventional wet coating procedures for graphite or Si/C. However, the lithium price is subject to large fluctuations.[14] Typically lithium foil is produced from an ingot

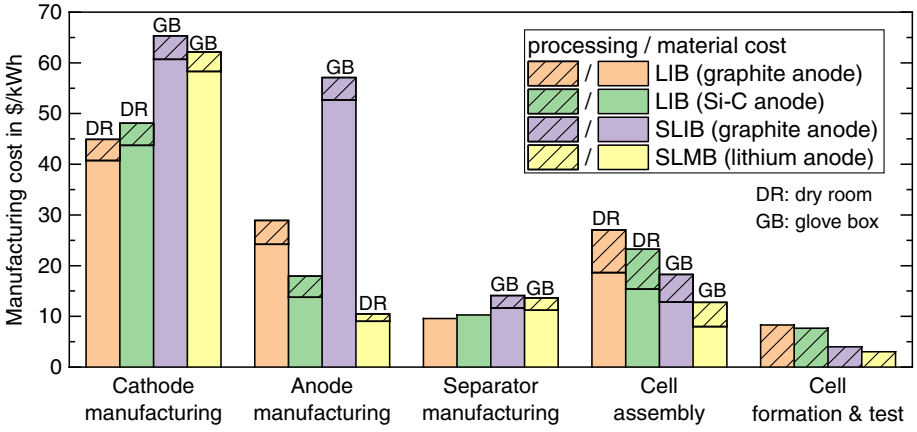

Figure 3. Material and processing cost for the different production stages corresponding to the scenarios presented in Figure 2.

© 2020 The Authors. Published by WILEY-VCH Verlag GmbH & Co. KGaA, Weinheim

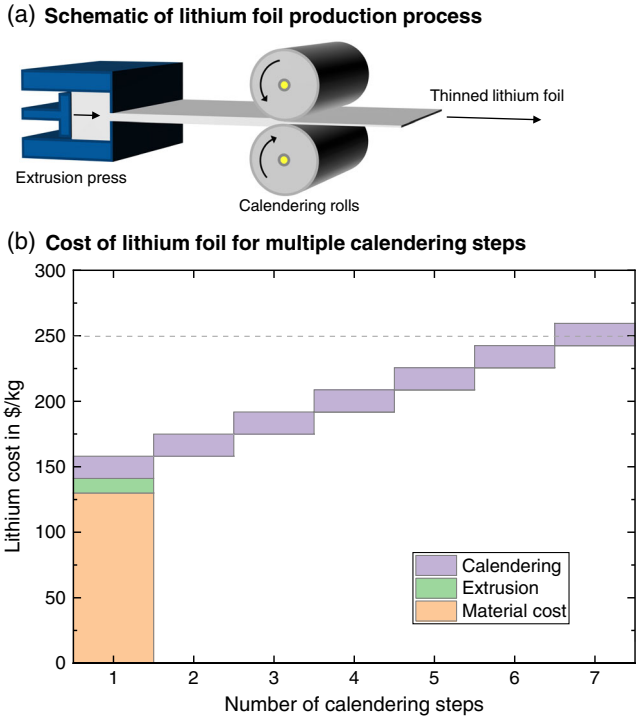

Figure 4. a) Schematic of the lithium foil production process. b) Cost of lithium foil for multiple calendering steps at a production output corresponding to 6 GWh per year. The dashed horizontal line indicates the cost to purchase lithium foil externally.[14]

(50–130 $ kg^{-1})[14] by extrusion and subsequent calendering to achieve the desired thickness (**Figure 4**a). Rolling of lithium toward foil thicknesses below 50 µm is challenging as lithium is a very adhesive and reactive material.[30,34] Although calendering in one single step toward 20 µm thickness or lower seems possible by controlled detachment using processing aids, usually multiple calendering steps are applied.[34] Hence, cost for lithium foil has been estimated to range between 250 and 1000 $ kg^{-1}.[14] To estimate whether it is cheaper to produce lithium foil on-site or to buy the foil from an external supplier, the cost for lithium foil was estimated for a varying number of calendering steps. The corresponding input parameters are summarized in **Table 3**.

As illustrated in Figure 4b, the cost for extrusion add up to 11.1 $ kg^{-1} to the material cost (a pessimistic value of 130 $ kg^{-1} was assumed as material cost baseline for the lithium ingot), whereas each calendering step adds an additional 16.9 $ kg^{-1} due to larger investment, plant area, etc. Although, for instance, a second calendering step would increase the overall cost of the sulfide-based SLMB by 0.5% compared with single-step rolling, buying the foil externally at a price of 250 $ kg^{-1} (1000 $ kg^{-1}) would result in a cost increase of 3.3% (30%). Hence, an in-house production for up to six successive calendering steps would result in lower cost than buying the foil from an external supplier at a price of 250 $ kg^{-1}. This would also allow for direct further processing which could be beneficial from a quality perspective.[35,36] However, rolling lithium toward layer thicknesses below 50 µm becomes more difficult with each calendering step and requires specific processing know-how. Hence, one of the biggest challenges will be to find skilled personnel to operate the machines.

Table 3. Input process parameters for lithium extrusion and calendering, based on an expert interview with a lithium foil manufacturer and Schünemann.[13]

Parameter	Unit	Extrusion	Calendering
Tape speed	m min^{-1}	25	25
Operating width	mm	500	500
Investment per machine	$	950 000	1 380 000
Qualified workers per shift and machine		0.25	0.5
Average electrical power per machine	kW	10	10
Plant area per machine	m^2	10	24

2.3. Parallel versus Bipolar Stacking

To systematically analyze the production cost of ASSBs, a detailed investigation of the underlying process steps is mandatory. This holds particularly true for the cell stack configuration[37] which has a major influence on the layout of the process steps. Typically, for conventional LIBs, the single galvanic elements in a cell stack are connected in parallel, i.e., the overall cell capacity is increased by joining all anode and all cathode current collector foils, respectively. Hence, additional space is consumed inside the packaging for welding joints of the current collector foils and tabs (**Figure 5**a). In this configuration, every anode current collector (typically copper foil) is sandwiched between two anodes, and every cathode current collector (typically aluminum foil) is sandwiched between two cathodes (double-sided coating). One particular advantage of ASSBs could be the possibility for a bipolar stacking configuration,[38] similar to fuel cell stacks. Here, the anode of one galvanic cell and the cathode of the adjacent galvanic cell share the same (bipolar) current collector (Figure 5b). This leads to a serial connection inside the cell stack, accompanied by an increase in the cell voltage for each set of layers. In this configuration, the current is drawn only from the outermost layers of the stack. Hence, less space is required for the welding joints of current collector foils and tabs, leading to a better utilization of the available packaging space.

A direct comparison of the processing cost for a sulfide-based SLMB with parallel and bipolar stacking is given in Figure 5c (left and middle bars). Although the material costs are slightly lower for the bipolar stacked configuration (85.3 $ kWh^{-1}) due to the higher energy content per cell (only 16.8 million cells produced per year), the processing costs are significantly higher (21.0 $ kWh^{-1}). Main contributors to the processing costs of both parallel and bipolar stacking are the wet coating and the cell stacking process (Figure 5d), which is in good agreement with literature for conventional LIBs.[13,29] Although the fabrication steps for the sulfide-based bipolar stacked ASSB are similar to the parallel stacked ASSB, several important deviations need to be considered: In contrast to the double-sided coatings for parallel stacking, a single-sided casting/coating step is used for both the composite cathode and the SES layer on top of the cathode layer. This means, however, that twice as many

© 2020 The Authors. Published by WILEY-VCH Verlag GmbH & Co. KGaA, Weinheim

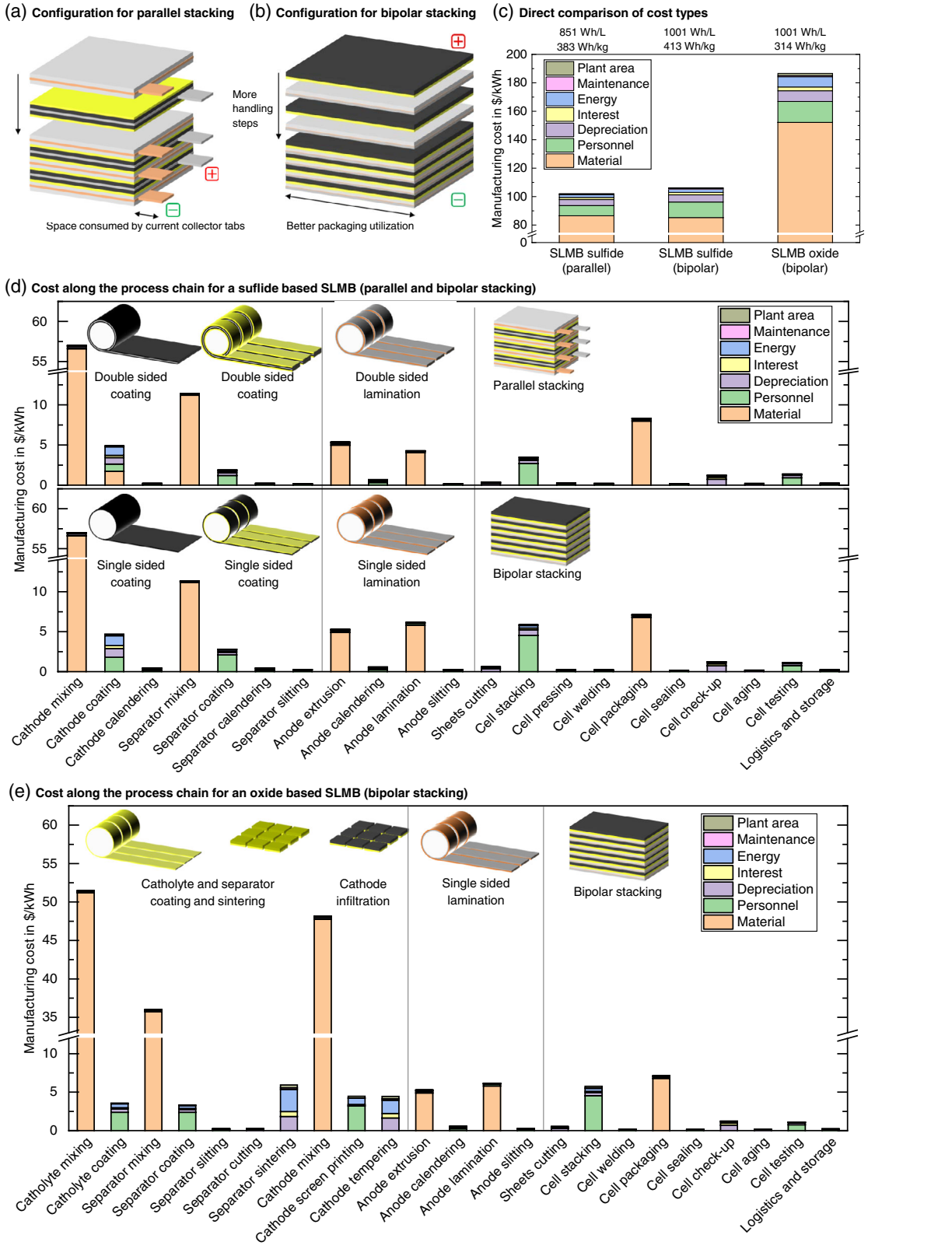

Figure 5. a) Cell stacking configurations for parallel and b) bipolar stacking. c) Direct comparison of manufacturing cost for sulfide- and oxide-based SLMB. Manufacturing cost along the process chains for d) sulfide- and e) oxide-based SLMB for a production output of 6 GWh year^{-1}.

© 2020 The Authors. Published by WILEY-VCH Verlag GmbH & Co. KGaA, Weinheim

coating (and calendering and slitting) machines will be required to produce the same amount of layers as for the parallel stacked cell with double-sided coatings. While the investment and power consumption for a single-sided coating machine are assumed to be significantly lower as for a double-sided coating machine (cf. Section 3), the required plant area and personnel cost will potentially be similar, i.e., the overall processing cost will be higher if twice as many machines are used. Furthermore, due to the asymmetric configuration, calendering of the composite cathode when combined with the bipolar current collector will most likely result in undesired strain which will seriously affect the succeeding processing steps.[24] Hence, it seems more plausible that the composite cathode is processed as a free-standing layer, for instance, by casting onto a carrier tape which will be removed during further processing. The bipolar current collector is therefore rather joined with the lithium anode (single-sided lamination). When comparing the configurations in Figure 5a, b, it becomes evident that also more cutting and handling steps will be required for the bipolar stacking configuration. Hence, more cutting and stacking machines will be required, further increasing the manufacturing cost. Of course, an additional lamination step could be applied for joining bipolar collector and composite cathode before stacking, thus reducing the number of handling steps.[37] However, this would result in further complications such as possible cross-contamination during sheet cutting. Note that the underlying SLMB cell configuration contains 141 single galvanic cells stacked in series, resulting in an average discharge voltage of 536 V. Additional cost for high-voltage safety measures during production were not taken into account for the calculation. Although the overall cell manufacturing cost for the bipolar configuration are higher (+4.1%) than for the parallel stacking configuration, the higher voltage allows to draw smaller currents from the cell, which could potentially result in cost savings on the battery module and pack level.

2.4. Sulfide versus Oxide Solid Electrolyte

Despite the high ionic conductivity of the sulfide-based SEs, their limited (electro)chemical stability is one of the main drawbacks.[16,39] In contrast, oxide-based SEs, such as LLZ, seem to be intrinsically stable against lithium metal[39] and also allow for high current cycling.[40] However, a high-temperature sintering step (>1000 °C)[17] is required to ensure sufficient ionic conductivity and proper densification of the SES. Due to expected complications for cosintering with cathode AMs,[41] the SES should be fabricated and sintered before joining with the electrodes. Sintered free-standing LLZ separator layers with relevant geometrical dimensions (layer thickness <100 μm, lateral area several tens of cm^2) do not have sufficient mechanical stability.[40] To circumvent these complications, a porous-dense LLZ bilayer has been suggested, fabricated by two tape-casting steps where one layer contains pore-formers to create the porosity during high-temperature sintering.[42] These pores are subsequently infiltrated with the cathode AM,[43] followed by a tempering step (cf. **Table 4**) at lower temperature (up to 700 °C).[44] Li_3BO_3 (LBO) has been suggested as a sintering aid for both SE and composite cathode.[44,45] Joining with the current collector can only take place after this step as the melting point of aluminum is below 600 °C. Hence, an additional handling or lamination step is required—independently on whether the cell is stacked in a parallel or bipolar configuration. Therefore, a bipolar stacking may indeed be more plausible for oxide-based ASSBs.

Table 4. Input parameters for LLZ separator sintering and composite cathode tempering, calculated based on the fully automated shuttle kiln for SOFC production by Scataglini et al.[46]

Parameter	Unit	Value [separator/cathode]
Parts per cycle		12 828
Time in oven	min	60
Time for loading/unloading	min	15
Investment per machine	$	2 200 000
Sintering temperature	°C	1000/700
Average electrical power per machine	kW	248/163
Plant area per machine	m^2	168
Variable scrap	%	10

When comparing the manufacturing cost of the oxide-based SLMB with the sulfide-based SLMB (bipolar stacking), a sharp increase in material cost (152.2 $ kWh^{-1}) and processing cost (34.5 $ kWh^{-1}) is evident (Figure 5c middle and right bars). As the volumetric composition was kept the same for all components, the higher density of LLZ (5.1 g cm^{-3}) compared to LPS (2 g cm^{-3})[18] results in a higher gravimetric SE content in the cathode (33.57 wt% LLZ vs 16.81 wt% LPS) and in the SES (97.82 wt% LLZ vs 97.44 wt% LPS). As the SE cost was held constant at 50 $ kg^{-1} for both LPS and LLZ, a higher gravimetric SE content in the SLMB will lead to higher overall material cost. Furthermore, as shown in Figure 5e, the separator sintering and cathode tempering steps significantly contribute to the processing cost. In particular, the energy cost and the depreciation are dominating, resulting from the high sintering temperature and investment, respectively. Note that also the scrap during tempering and sintering leads to a higher material cost.

In particular, the SE material cost is currently among the great unknowns for ASSB production. To analyze the influence on the overall manufacturing cost, SE material costs were varied from 100 to 10 $ kg^{-1} for both LPS (sulfide-based SLMB) and LLZ (oxide-based SLMB). The resulting manufacturing cost for the bipolar stacking configuration are shown in **Figure 6**. The vertical dash-dotted line corresponds to the LIB with Si/C anode (cf. Figure 2) The manufacturing cost for the sulfide-based SLMB vary from 132 to 86 $ kWh^{-1}, with a "break-even" for the LIB with Si/C anode at ≈50 $ kg^{-1} LPS. Due to its higher density, the price of LLZ has a stronger influence on the overall manufacturing cost, indicated by the steeper slope (from 267 to 123 $ kWh^{-1}). The analysis also shows that even if the LLZ cost could be pushed toward 10 $ kg^{-1}, manufacturing cost on the cell level will not be competitive with the LIB with Si-C anode. Nonetheless, the oxide-based SLMB could be a viable option in applications where other factors (e.g., energy density or safety) are more relevant than cost. Further cost savings potential lies on the battery module and pack level, for instance, if efforts for safety management can be reduced.

© 2020 The Authors. Published by WILEY-VCH Verlag GmbH & Co. KGaA, Weinheim

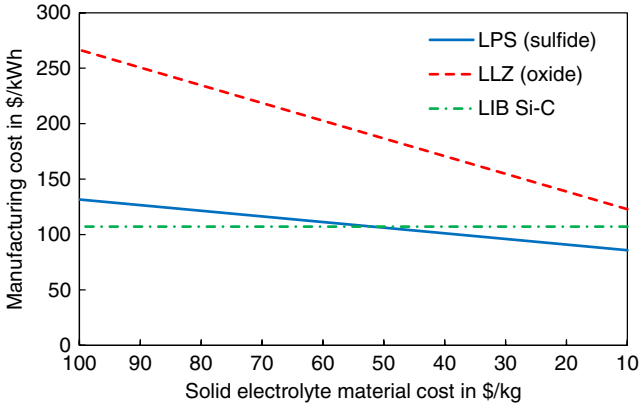

Figure 6. Manufacturing cost for varying SE material prices for sulfide- and oxide-based SLMB with bipolar stacking configuration and a production output of 6 GWh per year.

2.5. Sensitivity—Inert Gas for Sulfides versus Sintering for Oxides

Due to the large number of input parameters (>200 input parameters per process chain), a sensitivity analysis of the cost model was carried out. Hereby, all input parameters were systematically varied by setting one individual parameter to +10% while keeping all other parameters constant and calculating the resulting manufacturing cost. Note that the model is neither symmetric nor linear, i.e., a reduction by −10% will not give the opposite result (similar considerations apply for a variation of ±5%, ±20%, etc.). The parameters with the highest impact (upper 15%) on the manufacturing cost for a bipolar stacked sulfide-based and oxide-based SLMB (cf. Figure 2) are shown in **Figure 7**a. As to be expected from existing LIB cost models, the model is most sensitive to material and cell design parameters, in particular, the cathode properties: Especially a higher cathode voltage and specific capacity would result in a significant cost decrease,[47] followed by the share of AM in the cathode, the cathode coating thickness,[48] and the cathode AM density. For the sulfide-based SLMB, an increase in cathode AM price leads to the highest rise in cost, as also predicted by literature on conventional LIBs.[49] This will be of particular interest if protective coatings are applied on the cathode: Assuming a 10% rise in cathode AM price, for instance by applying a core-shell coating with ZrO_2,[50] the overall SLMB cost will increase by 3.2%. For the oxide-based SLMB, the SE price and the share of SE in the cathode have an even higher impact. This can be attributed to the fact that the LLZ density is even higher than the density of NMC 811 (cf. Table S2, Supporting Information). Also an increase in the separator thickness or the anode balancing factor (corresponding to the anode thickness) results in a higher price, which could be of particular interest if additional protective layers are used.[25,42] Further important cell design parameters are, among others, the cell housing dimensions.[51] Interestingly, a 10% increase in anode AM price (i.e., the price for a lithium ingot) would only result in a cost increase of 0.26% to 0.46%. Unsurprisingly, the general parameters with the highest impact on the cell manufacturing cost are labor related (working hours and salary).[52] Furthermore, the machine availability plays a significant role as a better machine utilization would allow to install less machines along the whole production line. For the processing parameters, the cathode slurry solids content has the highest impact on the manufacturing cost, which is in good agreement with estimations for conventional LIB production.[32,53] Hence, replacing the wet coating process by a high-viscosity extrusion process[9] would result in a significant cost reduction if similar considerations for investment, throughput, and so on, were assumed. Among the other relevant processing parameters are in particular the stacking process (throughput and personnel) for the sulfide-based SLMB (cf. Figure 5d) and the sintering and tempering scrap rate for the oxide-based SLMB (cf. Figure 5e).

Unexpectedly, none of the inert gas housing parameters seem to play a relevant role in the processing cost for the sulfide-based SLMB. To investigate the influence of the inert gas parameters, a Monte Carlo simulation was carried through, allowing for simultaneous variation of multiple parameters (cf. Section 3). Figure 7b shows the resulting histograms for variations of the inert gas loss and inert gas price (upper image) and the cost for housing, gas purification, and vacuum locks (bottom image). The inlays show the input probability distributions, whereas the vertically dashed lines correspond to the direct calculation (without parameter variation). While the resulting battery cell price range for a variation in argon loss (0.025–0.10 vol% h^{-1}) and price (1.15–4.6 \$ m^{-3}) only lies within 106.0 and 106.6 \$ kWh^{-1}, cost deviations for enclosure (4820–19 280 \$ m^{-3}), gas purification (1525–6100 \$ m^{-3}), and vacuum locks (\$ 24 250 per piece to \$ 97 000 per piece) lead to a broader distribution (105.7–107.0 \$ kWh^{-1}). Of course, the associated technical issues with processing in argon atmosphere (intralogistics, work piece carriers, functionality of electric motors, etc.) have not been considered in the economic model and could result in further expenses. Nonetheless, the overall impact of the inert gas processing parameters on the manufacturing cost seems to be rather small with regard to other input parameters. In comparison, the sintering parameters for the oxide-based SLMB were varied. Figure 7c shows the resulting histograms for variations of the duration (upper image) and the scrap rate (bottom image) of the separator sintering and cathode tempering steps. A variation in sintering and tempering time between 0.5 h and 2 h results in a cost distribution between 183 and 191 \$ kWh^{-1}, while scrap rates between 5% and 20% would even result in cost variations between 176 and 208 \$ kWh^{-1}. Of course, higher scrap rates in one process step necessitate that all preceding process steps produce more parts. Hence, a reduction in scrap during sintering and tempering would enable to install less machinery for slurry mixing, tape casting, sheet cutting, etc. These results impressively show the strong influence of the sintering process on the overall manufacturing cost of oxide-based SLMBs, as also predicted in a recent top-down cost estimation.[15]

2.6. The ADM: A Promising Alternative?

To circumvent the critical sintering step, the ADM has been suggested as a promising alternative for oxide-based SLMBs.[15] The ADM allows to fabricate dense LLZ separator layers without the need for high-temperature sintering[54] by accelerating the

© 2020 The Authors. Published by WILEY-VCH Verlag GmbH & Co. KGaA, Weinheim

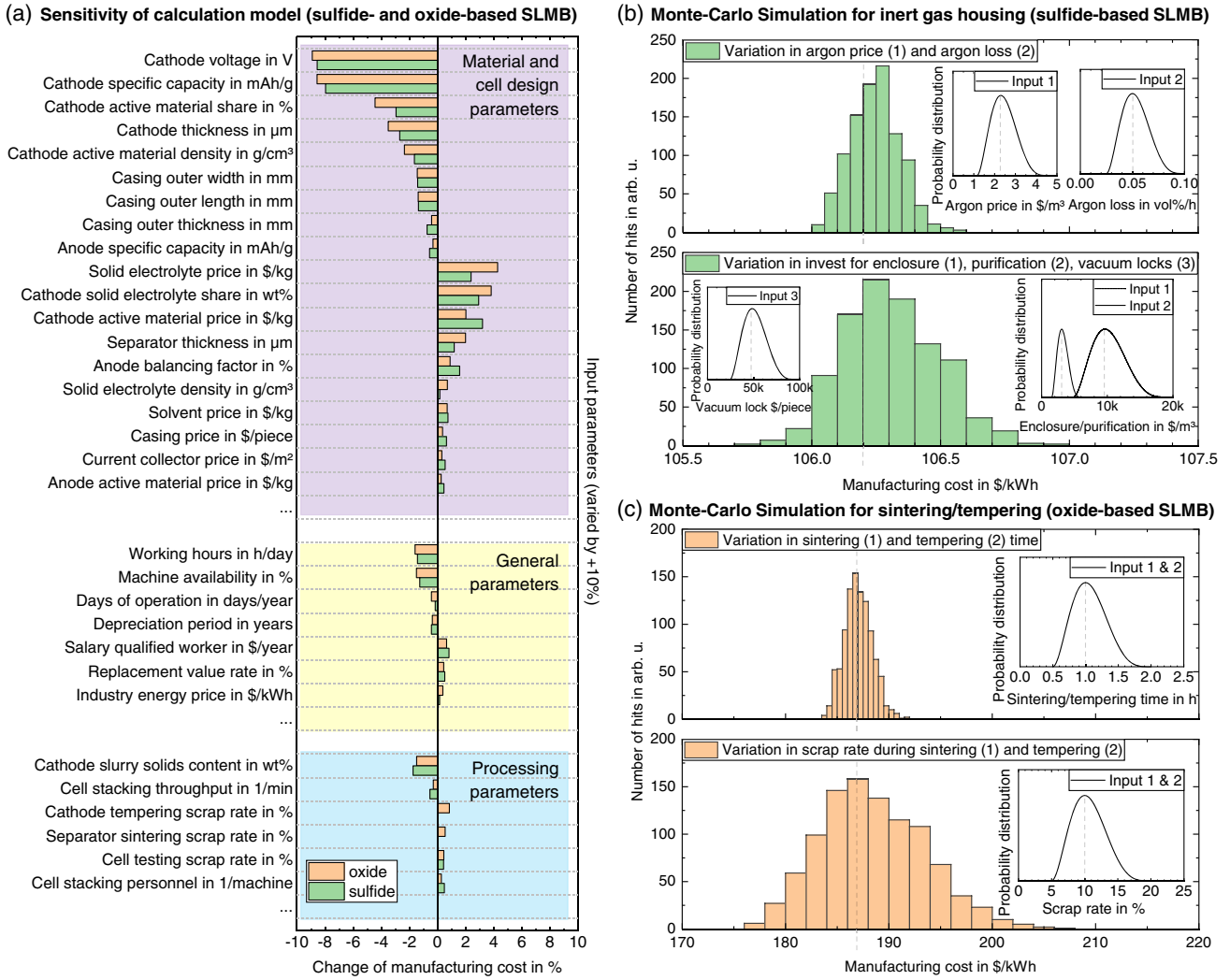

Figure 7. Sensitivity of the calculation model for sulfide-based and oxide-based SLMB (bipolar stacking). a) The upper 15% of all input parameters with the largest impact on the overall manufacturing cost for a systematic input parameter variation of +10% (cf. main text). b) (sulfide-based SLMB) shows the results of a Monte-Carlo Simulation for a variation in argon price and argon loss (upper image) and a variation in the average investment for inert gas enclosure, gas purification and vacuum locks (bottom image). c) (oxide-based SLMB) shows the results of a Monte Carlo simulation for a variation in separator sintering and cathode tempering time (upper image) and a variation in the scrap rate for separator sintering and cathode tempering (bottom image). The inlays in images (b) and (c) show the probability density distributions for the varied input parameters (cf. Section 3). The vertical dashed lines indicate the direct calculation (without variation). Each Monte Carlo Simulation was run 1000 times.

LLZ powder directly onto a substrate (e.g., the cathode composite) using a carrier gas stream[55] (**Figure 8**a). The ADM would enable to fabricate thinner separator layers (e.g., 5 µm)[54] and to combine different types of SE materials in cathode and separator layer.[56] This would allow for an improved cell design with reduced LLZ content, as shown in Figure 8b: Here, the energy density (in Wh L^{-1}, red dashed line) and the specific energy (in Wh kg^{-1}, blue lines) on the cell level (incl. PHEV 2 housing, bipolar stacking) are plotted as a function of the LLZ separator thickness. The dash–dotted blue line corresponds to an SLMB with LLZ as separator and catholyte, whereas the solid blue line corresponds to an SLMB with LLZ as separator but LATP as catholyte. While both energy density and specific energy decrease with thinner separator layers, the lower density of LATP ($2.9\,g\,cm^{-3}$) results in a higher specific energy: For instance, by replacing LLZ in the cathode with LATP and decreasing the separator layer thickness from 20 µm to 5 µm, the specific energy could be increased from 314 up to 405 Wh kg^{-1} (vertical gray bars). Despite the great potential of the ADM,[57] the technology is quite immature[15] and the deposition rate is currently limited to approximately $10\,mm^3\,min^{-1}$.[55] Hence, assuming a separator sheet area of $127\,cm^2$ and a separator thickness of 5 µm, the throughput would be limited to 0.157 sheets per minute (cf. **Table 5**). In comparison, a tape casting machine with a tape speed of $20\,m\,min^{-1}$ at a coating width of 600 mm can produce almost 1000 sheets per minute.

Figure 8c shows a rough estimation of the overall manufacturing cost for an improved cell design (LATP in the cathode) as a

© 2020 The Authors. Published by WILEY-VCH Verlag GmbH & Co. KGaA, Weinheim

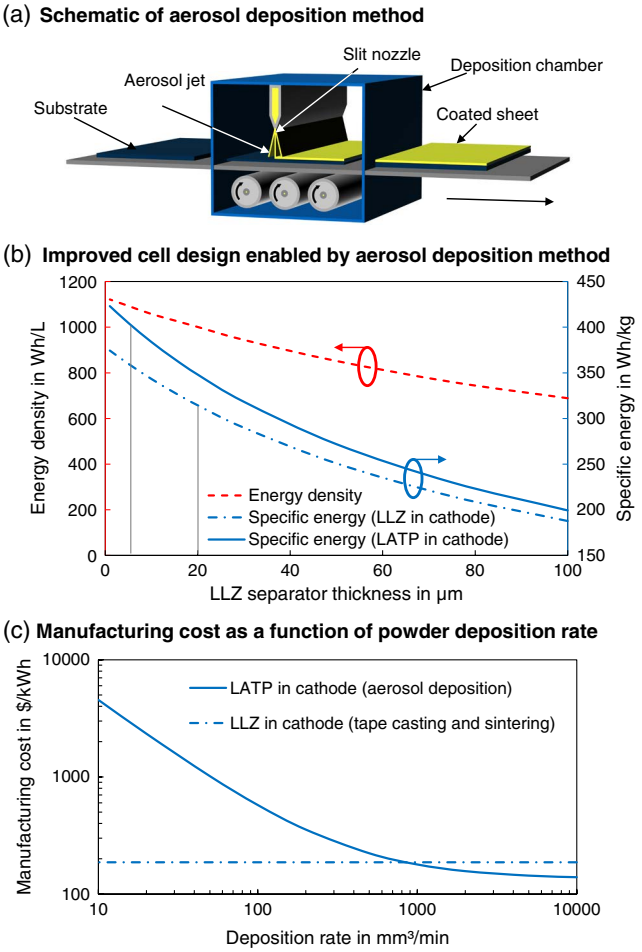

Figure 8. a) Functional principle of the ADM. b) Energy density and specific energy for a bipolar stacked oxide-based SLMB (incl. PHEV 2 housing) as a function of LLZ separator thickness for different catholytes. The vertical gray bars indicate the increase in specific energy for an improved cell design enabled by the ADM. c) Simplified estimation of the overall manufacturing cost for the improved cell design (5 µm thick LLZ separator produced by aerosol deposition, LATP as catholyte) as a function of the LLZ powder deposition rate for a production output of 6 GWh per year. The horizontal dash–dotted line corresponds to the reference scenario (20 µm thick LLZ separator produced by tape casting and sintering, LLZ as catholyte).

Table 5. Input process parameters for aerosol deposition, based on Helfritch et al.[58] and Hanft et al.[55] (cf. Section 3).

Parameter	Unit	Value
Deposition rate	$mm^3\ min^{-1}$	Variable (10–10 000)
Sheets per minute	min^{-1}	Variable (0.157–157)
Investment per machine	$	900 000
Qualified workers per shift and machine		1
Average electrical power per machine	kW	37.2
Plant area per machine	m^2	4.5
Powder to gas (N_2) rate	wt%	4.7
Nitrogen cost	$\$\ kg^{-1}$	0.14

function of the LLZ deposition rate for a 5 µm thick separator layer. Note that the calculation is based on simplified assumptions, i.e., material losses due to overspray and limited deposition efficiency were neglected and the investment, machine baseline area, power consumption, and nitrogen flow were held constant. The corresponding process chain was adapted from Schnell et al.;[15] all other process parameters are summarized in Supplementary Table S4, Supporting Information. The horizontal dash–dotted line corresponds to the oxide-based SLMB (cf. Figure 5) as a reference. Starting from the initial 10 $mm^3\ min^{-1}$ (0.157 sheets per minute), the overall manufacturing cost drop from over 4000 $\$\ kWh^{-1}$ and do not break even with the reference until a deposition rate of approximately 1000 $mm^3\ min^{-1}$ (15.7 sheets per minute) is reached. Of course, the number of aerosol deposition machines required to produce an output of 6 GWh per year can be drastically reduced by increasing the deposition rate. However, to achieve such high deposition rates, multi-nozzle systems with broad nozzles[59] and transport belts will be required.[60] This means, even higher throughputs will be required to account for the additional cost for increased gas flow, power consumption, and plant area cost for such a machine. The low maturity degree of the technology[15] will require additional cost for development which were not taken into account in the underlying model.

3. Methods

3.1. Calculation Logic

Due to its abstract calculation logic and the relatively transparent documentation of input parameters, the bottom-up cost model for LIB cell production by Schünemann[13] was used as a reference for the implemented calculation tool. Other established battery calculation models, such as Batpac,[61] also provide a sound basis for battery production cost estimation, but lack the flexibility required for comparison of different manufacturing processes and sequences. The input and output parameters for the cost model were stored as MS Excel sheets, whereas the calculation logic was implemented in MATLAB (version R2018 b), as illustrated in the UML diagram in Figure S1, Supporting Information. Depending on the process chain layout, the modeling tool requires a total number of approximately 200 input parameters per process chain which were gathered empirically based on literature values, expert interviews, and supplier quotations. To enable a certain comparability to other works in the field, most parameters were taken from literature values; however, some of which are based on data collected as early as 2011[48] and might be outdated. Furthermore, inflation and so on were not taken into account. Material prices, in particular, are subject to strong fluctuations and often depend on the negotiation position. Prices for machinery and equipment were mostly taken from literature, in some cases based on expert interviews with machine tool manufacturers, and, wherever possible, based on actual supplier quotations. Note that the names of the experts and companies cannot be published due to confidentiality reasons. Values given in EUR were transferred to USD at a currency exchange rate of 1.15 (10 Jan 2019).

© 2020 The Authors. Published by WILEY-VCH Verlag GmbH & Co. KGaA, Weinheim

For cost modeling, relevant cell parameters and general parameters are calculated, such as the anode thickness, the number of layers per cell stack, the energy content per cell, the number of cells produced per year, etc. In a second step, an iterative procedure for calculation of the single process steps is carried through. Considering the fixed scrap F and variable scrap v, the input I of each process can be calculated based on the required output O[13]

$$I = \frac{O}{1-v} + F \tag{1}$$

Starting from the total amount of cells produced per year, the input required for the final process step—typically the quality check—can be calculated. An iterative procedure is applied for a backward calculation along the whole process chain, based on the assumption that the output of each process step serves as input for the succeeding process. Hereby, the throughput of a single machine (in cell equivalents per unit time) is used to deduce the total number of machines per process step. Thus, the total amount of material and purchased parts can be determined, and the cost types (material, personnel, depreciation, etc.) can be attributed to each process step. Hence, considering additional cost such as logistics and storage, the overall cost for cell production can be calculated for the different scenarios. More details can be found in the cited reference.[13] Since the process steps for ASSBs can only be vaguely described up to date, fixed scrap was neglected in all scenarios. To verify the modeling tool, the parameter set suggested in Schünemann[13] was used to model the production of a conventional LIB cell in PHEV 2 format with a graphite anode and NMC 111 cathode, as shown in Figure S2, Supporting Information.

3.2. Modeling Parameters

An overview of the cell design parameters for the different scenarios is given in Table 1 and Table S1, Supporting Information. Material data can be found in Table S2, Supporting Information. The underlying general assumptions (availability of workforce, wages and salaries, financial aspects, plant floor and building, logistics and storage) are summarized in Table S3, Supporting Information. The process parameters for the different scenarios are summarized in Table S4, Supporting Information. The following section describes the underlying assumptions for the processes along the process chain of a conventional LIB based on Schünemann[13] and the reasons for parameter variations in the different scenarios.

3.2.1. Baseline Parameters

Mixing: A homogeneous slurry is prepared before wet coating. The amount of slurry to be mixed per cell for each component can be calculated based on the layer dimensions, the number of layers per cell, and the amount of solvent required to achieve the desired viscosity (typically, a solids content of 50–70% is targeted in LIB cell production.[23] For each component, the solvent mass required per ASSB cell is calculated via

$$m_{\text{solvent}} = \frac{n \cdot \sum m_i}{\varepsilon} \tag{2}$$

with n the number of layers, m_i the individual mass of the layers' constituents, and ε the solids content, which was set to 65% for all investigated scenarios. Note that different solvents were assumed for the different components: While for conventional cathodes with polyvinylidene fluoride (PVDF) binders, typically *N*-Methyl-2-pyrrolidone (NMP) is used as a solvent, water-based processing is common for graphite and Si/C anodes with SBR binders. In contrast, apolar solvents such as toluene are commonly used for sulfide-based SEs,[62] for instance in combination with acrylonitrile butadiene rubber (NBR).[63] Toluene has also been used for oxide-based slurries,[40] with LBO as a binder and sintering additive.[45] Carbon black (CB) is not only used as a CA in the cathode but can also be used as a pore former for fabrication of a porous sintered structure[64] (4 wt% of pore formers were assumed for the oxide-based catholyte slurry).[40]

Wet Coating/Tape Casting: The slurry is cast via a roll-to-roll process onto a current collector or a carrier foil. The thickness of the resulting layer is defined by the application tool, such as a doctor blade or slot dye. Subsequently, the solvent is evaporated in a drying tunnel which can consist of multiple drying chambers. The length of the drying tunnel l_{dryer} is determined by the targeted tape speed v_{tape} as

$$l_{\text{dryer}} = t_{\text{drying}} \cdot v_{\text{tape}} \tag{3}$$

where the drying time t_{drying} is estimated to be directly proportional to the amount of solvent per unit area[64]

$$t_{\text{drying}} \sim \frac{m_{\text{solvent}}}{A_{\text{coating}}} \tag{4}$$

This means, a thicker layer usually requires a longer drying tunnel if the coating speed is to be kept constant. Hence, the machine area, the power consumption, and the investment per machine need to be adjusted depending on the layer to be fabricated. Hereby, the machine area A_{machine} can be estimated as

$$A_{\text{machine}} = w_{\text{machine}} \times (l_{\text{coater}} + l_{\text{dryer}}) \tag{5}$$

where w_{machine} and l_{coater} are assumed to be 3 and 2 m, respectively.[13] The machine area was calculated individually for each ASSB cell design based on the empirically gathered values of Schünemann,[13] assuming a drying length of 36 m and 35 m for a solvent amount of 9.21 mg cm^{-2} NMP and 3.45 mg cm^{-2} water, respectively. For the process steps using toluene as a solvent, the evaporation rate was assumed to be similar to the one of NMP. The cost and power consumption of the drying tunnel were both assumed to scale linearly with the tunnel length, with a constant baseline offset for the coating unit.[13] Hence, also the cost and power for a two-story coating machine (for double-sided coatings) were assumed to be twice as high as for a single-sided coating machine.

Calendering: To reduce the layer porosity induced by the evaporated solvent, a calendering step is applied. Note that achieving close-to-zero porosities can be challenging[62] and fine tuning of process parameters will be required to reduce calendering induced defects such as embrittlement or corrugation.[24]

© 2020 The Authors. Published by WILEY-VCH Verlag GmbH & Co. KGaA, Weinheim

Nonetheless, the ductility of the sulfide-based SE may allow for negligible porosities by hot pressing at 150 °C.[65]

Slitting: Typically, the resulting broad coils are slit into several narrower coils to facilitate subsequent processing.

Intensive Drying: Before transferring the coated graphite and Si/C anodes into the dry room, water residuals are removed by an intensive drying step.

Cutting: Before cell assembly, the coils are typically cut to sheets with the final dimensions, for instance by laser cutting.[26] Hereby, the number of sheets to be cut is dependent on the amount of layers per cell and the configuration of the layers to be cut: For instance, the number of cutting steps is reduced for layers which are coated or laminated on top of each other (cf. Figure 2a). This could, however, lead to a higher risk of cross-contamination.

Stacking: The first step in cell assembly is the stacking of the individual layers. Similar to the cutting process, the number of handling steps is dependent on the layer configuration. A Z–folding process was assumed for the conventional LIBs with porous separator,[26] whereas single-sheet stacking seems more plausible for ASSBs. While the stacking speed is mainly limited by the acceleration of the electrode grippers, the investment for a single-sheet stacking machine will be lower due to the omission of the separator feeding unit with tension control and so on.

Tab Welding: After stacking, the anode and cathode current collectors are welded and joined with the current collector tabs or the lid. Typically, ultrasonic welding is employed.[29] As not much is known on contacting of the outer layers for a bipolar stacking configuration, the same parameters as for the parallel stacking were assumed.

Packaging and Sealing: Subsequently, the cell stack is placed into the housing which is then sealed with the lid (for hardcase cells, typically, a laser welding process is used).

Electrolyte Filling and Riveting: For conventional LIBs, the liquid electrolyte is injected into the cell to fill the pores in the electrodes and the separator. The process is decisive for the overall cell quality[36,66] and the subsequent wetting can be a bottleneck in cell production.[67]

Formation: During the formation procedure, the cells are charged for the first time. For the reference scenarios (LIB), one formation cycle (charge and discharge) is assumed at 0.1 C (20 h in total), followed by a check-up cycle at 0.5 C (4 h in total). Finally, the cells are charged up to 50% SOC at 0.5 C (1 h).[13] Although for ASSBs the formation step can potentially be omitted,[9,33] it is assumed that a check-up will be required anyways to ensure proper functionality and provide the required documentation for the customer. It is presumed that the investment for the formation channels (incl. auxiliaries) scales linearly with the battery cell capacity (in Ah), which is in accordance with quotations from cell testing equipment manufacturers. Note that for bipolar stacking, the voltage will increase with the number of layers per cell stack, whereas the capacity corresponds to the capacity of one single galvanic cell. Hence, a high-voltage testing equipment will be necessary, whereas much smaller currents will be required in comparison to parallel stacking. To facilitate comparability, the batteries' energy content (in Wh) was used to scale power consumption (taking into account the formation time and the number of cycles)[13] and investment.

Aging: After formation, the cells are typically stored in a controlled environment for several days up to several weeks, for instance to measure the self-discharge and to identify defective cells.[68]

Quality Check: In a final quality check, the cell voltage, the internal resistance, and the dimensional accuracy are controlled and the cells are graded according to quality.[13]

3.2.2. Other Process Parameters

The assumptions for process steps not covered in conventional LIB production will be described in the following (alphabetical order):

Aerosol Deposition: Due to the high uncertainty associated with the low maturity degree of the ADM,[15] obtaining reliable data was challenging. Machine parameters (invest, power consumption, personnel) for the ADM were taken from Helfritch et al.[58] and held constant for all calculations. The machine area was estimated based on Hanft et al.,[55] taking into account additional space required for continuous processing (conveyor belts, etc.). The number of sheets to be coated was calculated as a function of the deposition rate using geometrical considerations based on the sheet area and layer thickness, whereby a deposition rate of 10 $mm^3\ min^{-1}$ was assumed as the baseline.[55] Note that further parameters, such as overspray, deposition efficiency, and so on, were not taken into account for the calculation.

Anode Extrusion and Calendering: Please refer to Section 2.2.

Anode Lamination: To join the lithium foil with the current collector, a lamination unit is used. Parameters were taken from an expert interview with an equipment manufacturer.

Screen Printing: For the oxide-based SLMB, a screen printing process is assumed for the infiltration of the cathode slurry into the sintered porous LLZ matrix. Parameters were adapted from SOFC production,[46] with similar considerations for the solvent evaporation as for the wet coating/tape casting.

Sintering: Parameters for sintering and tempering of the oxide-based ASSB cells were adapted from the bottom-up calculation model for solid oxide fuel cell (SOFC) manufacturing by Scataglini et al.[46] The reference scenario is a fully automated shuttle kiln firing 4960 pieces ($181.5 \times 181.5\ mm^2$ per piece) at 1300–1400 °C for 24 h. Hence, the amount of sheets to be fired per cycle was calculated based on geometrical considerations, whereas the power consumption was assumed to scale linearly with the sintering temperature. A sintering temperature of 1050 °C and a sintering time of 1 h were assumed for the LLZ bilayer matrix,[40] whereas cofiring of the oxide-based cathode composites and annealing of the LLZ separator after ADM were assumed to take place at 700 °C for 1 h.[44,54]

Stack Pressing: The performance of sulfide-based ASSBs can be enhanced by stack pressing at increased temperature.[69] A uniaxial press with twelve pressing steps per minute was assumed, with a parallel processing of three cell stacks per pressing step. Parameters were gathered in an expert interview with a machine tool manufacturer.

3.3. Monte Carlo Simulation

For the Monte Carlo Simulation, a random value is generated for the input parameters to be varied. A beta function ($\alpha = 3, \beta = 5$)[70] was chosen as the probability density

© 2020 The Authors. Published by WILEY-VCH Verlag GmbH & Co. KGaA, Weinheim

distribution, the outline of which resembles the shape of a slightly asymmetric Gaussian distribution. However, the restricted domain (0–1) ensures non-negative values and the asymmetrical shape allows to take into account outliers. The beta distribution was renormalized such that the baseline value x represents the most likely value and 95% of all values lie within $x \pm \frac{x}{2}$. However, outliers can be accounted for by setting the upper boundary to $2 \times x$. The lower boundary was set to $\frac{x}{2}$. Each Monte Carlo Simulation was run with 1000 iterations.

4. Conclusion

In summary, a bottom-up calculation model was built to compare the manufacturing costs of various ASSBs cell designs with conventional LIBs. The model allows for a detailed investigation of the corresponding process chains and reveals that a sulfide-based SLMB could be produced at costs competitive even to future LIBs with Si/C anode. Among the main factors for cost savings are the omission of the electrolyte filling process and a simplified formation procedure. In contrast to common understanding in literature, processing in argon atmosphere does not seem to significantly increase the overall manufacturing cost compared to processing in a dry room. However, the technical issues associated with production in a glovebox environment could result in further complications. While buying lithium foil from an external supplier would result in higher cost, processing know-how and personnel will be decisive for economic in-house fabrication of lithium anodes. Although a bipolar stacking would enable an improved packaging utilization and higher battery cell voltage, the additional effort during processing might result in a higher manufacturing cost on the cell level. Due to the high density of LLZ and the high cost during sintering, an oxide-based SLMB will hardly be cost competitive, even if the LLZ price can be pushed towards 10 \$ kg^{-1}. This was confirmed also by a systematic sensitivity analysis and the subsequent Monte Carlo simulations. Despite the potential for improved cell design and significant reduction of the sintering temperature, much effort will be required to implement and industrialize the ADM as an alternative for SES fabrication. The results of this study will help research and development to mitigate the risks associated with the high uncertainty about ASSB cell design and processing of ASSB components. Further research should in particular validate the underlying assumptions by upscaling and investigating process parameters and resulting issues on a pilot and industrial scale.

Supporting Information

Supporting Information is available from the Wiley Online Library or from the author.

Acknowledgements

The authors express their gratitude to the German Federal Ministry of Education and Research (Bundesministerium für Bildung und Forschung) for financial support. Some of the results have been achieved within the scope of the research projects "FELIZIA" (grant number 03XP0026I) and "ProFeLi" (grant number 03XP0184I). The authors would also like to thank Florian Günter and Fabian Konwitschny for proof-reading of the manuscript.

Conflict of Interest

The authors declare no conflict of interest.

Keywords

all-solid-state batteries, battery production, cost analysis, economic evaluation, lithium-ion batteries

Received: October 18, 2019
Revised: December 18, 2019
Published online: January 16, 2020

[1] T. Inoue, K. Mukai, *ACS Appl. Mater. Interfaces* **2017**, *9*, 1507.
[2] J. Janek, W. G. Zeier, *Nat. Energy* **2016**, *1*, 16141.
[3] Y. Kato, S. Hori, T. Saito, K. Suzuki, M. Hirayama, A. Mitsui, M. Yonemura, H. Iba, R. Kanno, *Nat. Energy* **2016**, *1*, 16030.
[4] Y. Seino, T. Ota, K. Takada, A. Hayashi, M. Tatsumisago, *Energy Environ. Sci.* **2014**, *7*, 627.
[5] H. Aono, *J. Electrochem. Soc.* **1989**, *136*, 590.
[6] R. Murugan, V. Thangadurai, W. Weppner, *Angew. Chem. Int. Ed.* **2007**, *46*, 7778.
[7] S. Troy, A. Schreiber, T. Reppert, H.-G. Gehrke, M. Finsterbusch, S. Uhlenbruck, P. Stenzel, *Appl. Energy* **2016**, *169*, 757.
[8] K. Kerman, A. Luntz, V. Viswanathan, Y.-M. Chiang, Z. Chen, *J. Electrochem. Soc.* **2017**, *164*, A1731.
[9] J. Schnell, T. Günther, T. Knoche, C. Vieider, L. Köhler, A. Just, M. Keller, S. Passerini, G. Reinhart, *J. Power Sources* **2018**, *382*, 160.
[10] F. Hao, F. Han, Y. Liang, C. Wang, Y. Yao, *MRS Bull.* **2018**, *43*, 775.
[11] B. Nykvist, M. Nilsson, *Nat. Clim. Change* **2015**, *5*, 329.
[12] O. Schmidt, A. Hawkes, A. Gambhir, I. Staffell, *Nat. Energy* **2017**, *2*, 17110.
[13] J.-H. Schünemann, *Modell zur Bewertung der Herstellkosten von Lithiumionenbatteriezellen*, Sierke, Göttingen **2015**.
[14] R. Schmuch, R. Wagner, G. Hörpel, T. Placke, M. Winter, *Nat. Energy* **2018**, *3*, 267.
[15] J. Schnell, F. Tietz, C. Singer, A. Hofer, N. Billot, G. Reinhart, *Energy Environ. Sci.* **2019**, *12*, 1818.
[16] H. Muramatsu, A. Hayashi, T. Ohtomo, S. Hama, M. Tatsumisago, *Solid State Ionics* **2011**, *182*, 116.
[17] Y. Li, J.-T. Han, C.-A. Wang, H. Xie, J. B. Goodenough, *J. Mater. Chem.* **2012**, *22*, 15357.
[18] T. Placke, R. Kloepsch, S. Dühnen, M. Winter, *J. Solid State Electrochem.* **2017**, *21*, 1939.
[19] DIN, *Electrically Propelled Road Vehicles – Battery Systems – Design Specifications for Lithium-Ion Battery Cells*, Beuth, Berlin **2016**.
[20] M. N. Obrovac, V. L. Chevrier, *Chem. Rev.* **2014**, *114*, 11444.
[21] W.-J. Zhang, *J. Power Sources* **2011**, *196*, 13.
[22] M. Wentker, M. Greenwood, J. Leker, *Energies* **2019**, *12*, 504.
[23] T. Günther, N. Billot, J. Schuster, J. Schnell, F. B. Spingler, H. A. Gasteiger, *AMR* **2016**, *1140*, 304.
[24] T. Günther, D. Schreiner, A. Metkar, C. Meyer, A. Kwade, G. Reinhart, *Energy Technol.* **2019**, *5*, 1900026.
[25] T. Ates, M. Keller, J. Kulisch, T. Adermann, S. Passerini, *Energy Storage Mater.* **2019**, *17*, 204.
[26] J. Kurfer, M. Westermeier, C. Tammer, G. Reinhart, *CIRP Annals* **2012**, *61*, 1.

© 2020 The Authors. Published by WILEY-VCH Verlag GmbH & Co. KGaA, Weinheim

[27] T. Knoche, G. Reinhart, *AMM* **2015**, *794*, 11.
[28] R. Jung, R. Morasch, P. Karayaylali, K. Phillips, F. Maglia, C. Stinner, Y. Shao-Horn, H. A. Gasteiger, *J. Electrochem. Soc.* **2018**, *165*, A132.
[29] A. Kwade, W. Haselrieder, R. Leithoff, A. Modlinger, F. Dietrich, K. Droeder, *Nat. Energy* **2018**, *3*, 290.
[30] H. C. Meyer, in *Handling And Uses Of The Alkali Metals*, Vol. *19*, American Chemical Society, Washington, DC **1957**, p. 9.
[31] S. Ahmed, P. A. Nelson, D. W. Dees, *J. Power Sources* **2016**, *326*, 490.
[32] D. L. Wood, J. Li, C. Daniel, *J. Power Sources* **2015**, *275*, 234.
[33] U. Grape, SEEO Final Technical Report: Recovery Act – Solid State Batteries for Grid-Scale Energy Storage **2015**, https://www.smartgrid.gov/files/Seeo_SolidStateBatteries_FTR_DE-OE0000223_0.pdf, (accessed: December 2019).
[34] P. Bouchard, P. E. Guerin, G. St-Amant, G. Laroche, *EP0692831B*, **1994**.
[35] J. Schnell, G. Reinhart, *Proc. CIRP* **2016**, *57*, 568.
[36] J. Schnell, C. Nentwich, F. Endres, A. Kollenda, F. Distel, T. Knoche, G. Reinhart, *J. Power Sources* **2019**, *413*, 360.
[37] F. Konwitschny, J. Schnell, G. Reinhart, *Proc. CIRP* **2019**, *81*, 1236.
[38] Y.-S. Hu, *Nat. Energy* **2016**, *1*, 16042.
[39] Y. Zhu, X. He, Y. Mo, *ACS Appl. Mater. Interfaces* **2015**, *7*, 23685.
[40] G. T. Hitz, D. W. McOwen, L. Zhang, Z. Ma, Z. Fu, Y. Wen, Y. Gong, J. Dai, T. R. Hamann, L. Hu, E. D. Wachsman, *Mater. Today* **2019**, *22*, 50.
[41] L. Miara, A. Windmüller, C.-L. Tsai, W. D. Richards, Q. Ma, S. Uhlenbruck, O. Guillon, G. Ceder, *ACS Appl. Mater. Interfaces* **2016**, *8*, 26842.
[42] K. Fu, Y. Gong, G. T. Hitz, D. W. McOwen, Y. Li, S. Xu, Y. Wen, L. Zhang, C. Wang, G. Pastel, J. Dai, B. Liu, H. Xie, Y. Yao, E. D. Wachsman, L. Hu, *Energy Environ. Sci.* **2017**, *10*, 1568.
[43] Y. Ren, T. Liu, Y. Shen, Y. Lin, C.-W. Nan, *Ionics* **2017**, *23*, 2521.
[44] D. Wang, Q. Sun, J. Luo, J. Liang, Y. Sun, R. Li, K. Adair, L. Zhang, R. Yang, S. Lu, H. Huang, X. Sun, *ACS App. Mater. Interfaces* **2019**, *11*, 4954.
[45] R.-H. Shin, S.-I. Son, S.-M. Lee, Y. S. Han, Y. D. Kim, S.-S. Ryu, *J. Korean Ceram. Soc.* **2016**, *53*, 712.
[46] R. Scataglini, A. Mayyas, M. Wei, S. H. Chan, T. Lipman, D. Gosselin, A. D'Alessio, H. Breunig, W. G. Colella, B. D. James, *A Total Cost Of Ownership Model For Solid Oxide Fuel Cells In Combined Heat And Power And Power-Only Applications*, Ernest Orlando Lawrence Berkeley National Laboratory, Berkeley **2015**.
[47] S. Ahmed, S. E. Trask, D. W. Dees, P. A. Nelson, W. Lu, A. R. Dunlop, B. J. Polzin, A. N. Jansen, *J. Power Sources* **2018**, *403*, 56.
[48] G. Patry, A. Romagny, S. Martinet, D. Froelich, *Energy Sci. Eng.* **2015**, *3*, 71.
[49] A. Sakti, J. J. Michalek, E. R. H. Fuchs, J. F. Whitacre, *J. Power Sources* **2015**, *273*, 966.
[50] N. Machida, J. Kashiwagi, M. Naito, T. Shigematsu, *Solid State Ion.* **2012**, *225*, 354.
[51] R. E. Ciez, J. F. Whitacre, *J. Power Sources* **2017**, *340*, 273.
[52] R. J. Brodd, C. Helou, *J. Power Sources* **2013**, *231*, 293.
[53] J.-H. Schunemann, H. Dreger, H. Bockholt, A. Kwade, *ECS Trans.* **2016**, *73*, 153.
[54] D. Hanft, J. Exner, R. Moos, *J. Power Sources* **2017**, *361*, 61.
[55] D. Hanft, J. Exner, M. Schubert, T. Stöcker, P. Fuierer, R. Moos, *J. Ceram. Sci. Technol* **2015**, *6*, 147.
[56] Y. Iriyama, M. Wadaguchi, K. Yoshida, Y. Yamamoto, M. Motoyama, T. Yamamoto, *J. Power Sources* **2018**, *385*, 55.
[57] A. Hofer, J. Schnell, B. Beck, G. Reinhart, *Proc. CIRP* **2019**, *81*, 1400.
[58] D. Helfritch, O. Stier, J. Villafuerte, in *Modern Cold Spray*, Vol. *17* (Ed: J. Villafuerte), Springer International Publishing, Cham, Switzerland **2015**, p. 377.
[59] H. Bae, J. Choi, G. M. Choi, *Solid State Ionics* **2013**, *236*, 16.
[60] T. Arndt, *US20130123112A1*, **2013**.
[61] P. A. Nelson, K. G. Gallagher, I. d. Bloom, D. W. Dees, *Modeling The Performance And Cost Of Lithium-Ion Batteries For Electric-Drive Vehicles* 2nd ed, Argonne National Laboratory, Argonne **2012**.
[62] N. Riphaus, P. Strobl, B. Stiaszny, T. Zinkevich, M. Yavuz, J. Schnell, S. Indris, H. A. Gasteiger, S. J. Sedlmaier, *J. Electrochem. Soc.* **2018**, *165*, A3993.
[63] K. Lee, S. Kim, J. Park, S. H. Park, A. Coskun, D. S. Jung, W. Cho, J. W. Choi, *J. Electrochem. Soc.* **2017**, *164*, A2075.
[64] R. Scataglini, M. Wei, A. Mayyas, S. H. Chan, T. Lipman, M. Santarelli, *Fuel Cells* **2017**, *17*, 825.
[65] D. H. Kim, D. Y. Oh, K. H. Park, Y. E. Choi, Y. J. Nam, H. A. Lee, S.-M. Lee, Y. S. Jung, *Nano Lett.* **2017**, *17*, 3013.
[66] F. J. Günter, C. Burgstaller, F. Konwitschny, G. Reinhart, *J. Electrochem. Soc.* **2019**, *166*, A1709.
[67] T. Knoche, V. Zinth, M. Schulz, J. Schnell, R. Gilles, G. Reinhart, *J. Power Sources* **2016**, *331*, 267.
[68] R. Petri, T. Giebel, B. Zhang, J.-H. Schünemann, C. Herrmann, *Int. J. Precis. Eng. Manuf.-Green Tech.* **2015**, *2*, 263.
[69] M. Yamamoto, Y. Terauchi, A. Sakuda, M. Takahashi, *Sci. Rep.* **2018**, *8*, 1212.
[70] K.-H. Waldmann, W. Helm, *Simulation stochastischer Systeme: Eine anwendungsorientierte Einführung*, Springer Gabler, Berlin **2016**.

© 2020 The Authors. Published by WILEY-VCH Verlag GmbH & Co. KGaA, Weinheim